LOCAL AND INTEGRAL PARAMETERS OF SWIRLING FLOW IN A LONG TUBE

A. A. Khalatov, V. K. Shchukin, and V. G. Letyagin

UDC 532.551

The behavior of isothermal flow in a tube of length 150 diameters is investigated for a wide range of intensities of the initial swirl.

Swirling flow is widely used in organizing and intensifying working processes in aviation and rocket technology and elsewhere. At present, the properties of the heat and mass transfer and hydraulic drag of swirling flows have been investigated in sufficient detail for relatively short channels ($\bar{x} < 15$) [1, 2], but to date there has not been adequate study of the flow in long tubes and the transition from swirling to axial flow. Literature data from analytic [3, 4], numerical [5], and experimental [6-9] investigations are not yet such as to allow unequivocal formulation of the main local and integral properties of swirling flow, which hinders the development of semiempirical and engineering methods of calculation.

In view of this, the present work has the following aims: to study the variation of the local and integral flow parameters in a tube of length 150 diameters over a wide range of intensities of the initial swirl; to investigate the properties of the flow at the wall; to determine the laws describing the damping of the initial swirl and the transition to axial flow; and to generalize the results obtained on the basis of a universal swirl parameter.

1. Experimental Apparatus

The experiments were carried out in a specially designed and constructed test stand consisting of an aerodynamic tube of open type; the working part was a cylindrical channel of diameter 80 mm and length 150 diameters. The velocity and pulsations were measured using a T7N thermoanemometer and the pressure was measured by miniature pneumometric sensors. The positioning device had two degrees of freedom and the accuracy of the radial positioning was 0.01 mm. The measurement cross sections were at $\bar{x}$ = 1, 4, 7, 10, 20, 40, 60, 80, 100, 120, and 145 diameters from the source of swirling. The Reynolds number Re_d varied from $0.5 \cdot 10^5$ to $1.5 \cdot 10^5$ in the experiments.

The initial swirl was produced by a bladed eddy generator with a central hub of diameter 37 mm. The blade shape corresponded to swirl given by the power law: $\tan \varphi = \tan \varphi_I (R/r)^n$. In the experiments φ_I varied from 15 to 60°; n, from −1 to 3. Altogether, eight eddy generators were studied.

The integral estimate of the initial swirl was made using the parameter Φ_{*in}, the ratio between the rotational and axial momenta of the flow. The relation between the calculated and mean experimental values was obtained experimentally and takes the form of a power law:

$$\tilde{\Phi}_{*in} = 0.56\,\Phi_{*in.c}^{0.75}. \quad (1)$$

Equations for $\Phi_{*in.c}$ are given in [10, 11].

2. Local Flow Parameters

Typical curves of the variation of the axial and rotational components of the velocity over the channel cross section are shown in Fig. 1. The variation in the total velocity resembles the axial-velocity distribution, but is characterized by a sharper radial gradient.

Translated from Inzhenerno-Fizicheskii Zhurnal, Vol. 33, No. 2, pp. 224-232, August, 1977. Original article submitted February 7, 1977.

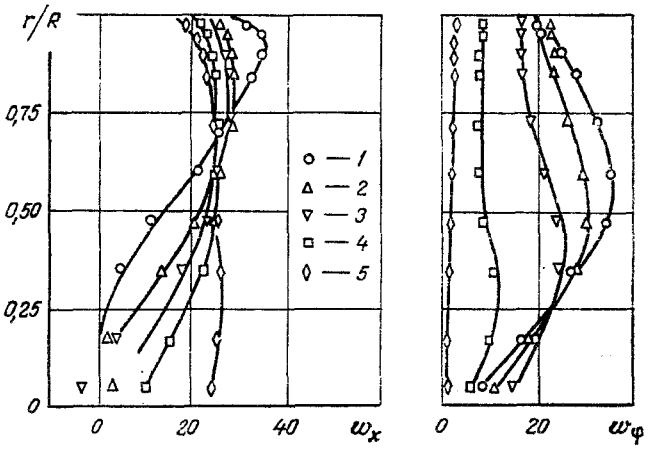

Fig. 1. Variation of w_x and w_φ (m/sec) over the length of the tube. Eddy generator parameters: $\varphi_I = 45°$, n = 3; $Re_d = 10^5$; 1) $\bar{x}$ = 1.05; 2) 7.05; 3) 20; 4) 60; 5) 145.

Analysis of the experimental data for all the eddy generators leads to the following basic conclusions, which are fairly general properties of swirling flows in a cylindrical channel for wide variation of the parameters and form of the initial swirl.

In the initial sections, where the swirl intensity is large, the bulk flow velocity (axial and total) at the channel surface considerably exceeds the mean flow rate and at the axis there appears a still region, characteristic for flow behind a streamlined body, or inverse flow. With increasing distance from the inlet, as a result of damping of the swirl, the bulk velocity decreases at the wall and rises at the axis; in the outlet cross section of the tube the distribution of w_x and w_Σ approximates to flow at the end of the hydrodynamic initial section.

If the experimental data are generalized, the following relations are obtained for the maximum axial and total densities of the bulk flow rate:

$$\frac{\rho_0 w_{x0}}{\rho u} = 0.95 + \frac{1.8\Phi_*^{0.81}}{Re_d^{0.12}}; \quad \frac{\rho_0 w_{\Sigma 0}}{\rho u} = 0.74 + \frac{5.75\Phi_*^{0.81}}{Re_d^{0.12}},$$

which apply when $\Phi_* > 0.23$. When $0 < \Phi_* < 0.23$, $\rho_0 w_{x0}$ and $\rho_0 w_{\Sigma 0}$ rise to the values characteristic of axial stabilized flow, as a result of the displacing effect of the boundary layer and the shift of the maxima $\rho_0 w_{x0}$ and $\rho_0 w_{\Sigma 0}$ in the region of the channel axis.

The relative radius of the axial region of inverse flow for the eddy generators investigated is given by the equation

$$\frac{r_{if}}{R} = 0.31(\Phi_*^{0.81} - 0.293)^{0.54},$$

and hence it follows that no inverse flow appears in the channel when $\Phi_* < 0.22$.

The distribution of the tangential component w_φ across the channel cross section has a maximum. With increase in φ_I and n the radius corresponding to the maximum rotational velocity $r_{\varphi\,max}$ is shifted toward the channel surface, while with damping of the swirl the maximum approaches the channel axis. In general, the following regions of flow are observed:

$\Phi_* > 0.5$: the distribution of w_φ has a clearly expressed maximum given by

$$\frac{r_{\varphi max}}{R} = 0.19 + 0.38\Phi_*;$$

$0.17 < \Phi_* < 0.5$: the change to quasisolid rotation begins; w_φ decreases considerably more rapidly near the maximum than at the surface, and so the distribution of w_φ does not have the usual maximum; i.e., under these conditions the limiting value $r_{\varphi\,max}/R$ is 0.35;

$\Phi_* < 0.17$: the distribution of w_φ practically corresponds to quasisolid rotation.

Note that in the ranges of Re_d, φ_I, and n considered, no region of potential rotation ($w_\varphi r$ = const) is observed at the channel surface; it can only be assumed that under conditions

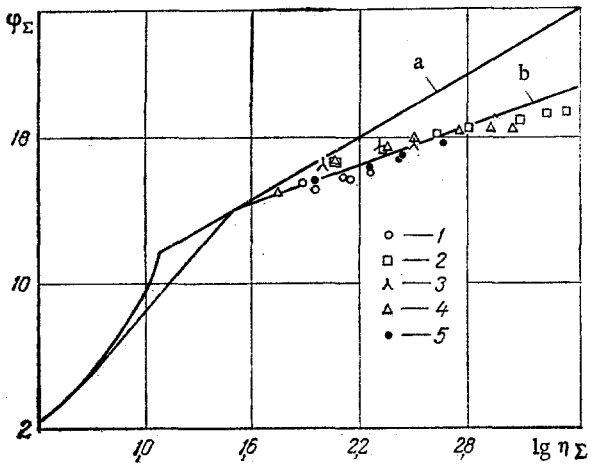

Fig. 2. Universal velocity distribution in the flow region at the wall: $\Phi_* = 0.2$; 1) $\varphi_I = 45°$, n = −1; 2) 45°, 3; 3) 45°, 1; 4) 15°, 3; 5) 30°, 3; a) $\varphi = 5.5 + 5.75 \log \eta$; b) $\varphi_\Sigma = 8.5 + 1.6 \log \eta_\Sigma$.

of significant swirl the variation of w_φ is close to potential rotation. In all cases, the maximum circulation of the rotational velocity is close to the wall, right up to the cross section in which the swirl is practically degenerate.

The total pressure P* and excess static pressure P in the flow correspond to complex variation of w_x and w_φ over the channel cross section. Outside the flow region at the wall, the radial gradient of the static pressure is determined by the equation of radial equilibrium, which leads to the approximate equation

$$P_w - P_{00} = \int_0^R \rho \frac{w_\varphi^2}{r}\, dr \quad \text{or} \quad \frac{dP_w}{dx} - \frac{dP_{00}}{dx} = \frac{d}{dx}\int_0^R \rho \frac{w_\varphi}{r}\, dr;$$

i.e., the longitudinal pressure gradient dP_w/dx is less at the surface than at the axis of the channel.

With damping of the swirl, the distributions of P and P* over the cross section are equalized and the region with approximately constant P* extends continuously to the channel axis. At the channel outlet the pressure distribution corresponds to that for the flow in the initial section of the tube.

Analysis of the experimental data for all the eddy generators leads to the following equations characterizing the surfaces of zero excess static and total pressures:

$$\frac{r_z}{R} = -0{,}12\,\Phi_*^{1.62} + 0.543\,\Phi_*^{0.81} - 0.14;$$

$$\frac{r_z^*}{R} = -0.11\Phi_*^{1.62} + 0.505\,\Phi_*^{0.81} - 0.13.$$

These equations apply when $\Phi_* > 0.23$. When $\Phi_* < 0.23$, there is no rarefaction in the channel.

Because the variation of w_x, w_φ, and w_Σ over the channel section is continuous, there is no boundary-layer region with predominant variation in velocity. Separation of a boundary layer and a potential core is only possible when the swirl is relatively weak (practically degenerate). Therefore, in deriving the integral momentum relations for swirling flow, the equations of motion were integrated between the limits 0 and R.

Analysis of the local properties shows that swirling flow in a cylindrical channel may be regarded as complex gasdynamic flow: In the flow region at the wall the gradients of the axial velocity and static pressure are negative, while at the axis they are positive. With damping of the flow, the region of inverse flow (or the still region) vanishes, and there is continuous withdrawal of mass in the axial region, initially because of decrease in the radial pressure gradient and then because of the growth of the boundary layer. Engineering methods of calculation must take these properties of the flow into account.

TABLE 1. Numerical Values of the Initial Swirl Intensity and the Limiting Value $\bar{x}_1$ for the Eddy Generators

	$\varphi_I=15°$, $n=3$	$\varphi_I=30°$, $n=3$	$\varphi_I=45°$, $n=3$	$\varphi_I=60°$, $n=3$	$\varphi_I=45°$, $n=1$	$\varphi_I=45°$, $n=0$	$\varphi_I=45°$, $n=1$	$\varphi=45°$, straight blades
$\tilde{\Phi}_{*in}$	0,384	0,486	0,826	1,23	0,433	0,592	0,69	1,29
$\bar{x}_1$	7	10	20	10	20	10	20	20

3. Flow Region at the Wall

The velocity distribution close to the channel surface is an important factor in heat- and mass-transfer processes. Analysis of several types of swirling flow (in cyclones and eddy generators, and on the convex surface of a curvilinear channel) shows that close to the surface the velocity distribution is logarithmic in form [2], but lies below the distribution characteristic of axial stabilized flow in the tube.

Analysis of the data of the present experiments shows that the variation of w_x and w_Σ at the wall is described by a power law with index 1/10-1/13. Since the velocity of the flow around the surface is w_Σ under the conditions considered, the parameters φ_Σ and η_Σ are chosen as universal coordinates, while the dynamic velocity v_Σ^* is determined from the variation of the integral flow parameters over the length of the channel (see Sec. 5).

Analysis of measurements in the region of axial stabilized flow shows that, for the conditions considered, the effect of the wall does not lead to any error in the measurements when $\eta_\Sigma \geq 50$. Accordingly, readings in the swirling flow were taken only in the region $\eta_\Sigma > 50$ when $\bar{x} > 15$.

Because the variation of w_Σ and w_x over the channel cross section is continuous, the logarithmic region will be called the flow region at the wall. Appropriate treatment of the experimental results leads to the equation

$$\varphi_\Sigma = (5.5 + 10.7\,\Phi_*^{0.81}) + (2.5 - 3.14\,\Phi_*^{0.81}) \ln \eta_\Sigma,\ \eta_\Sigma > 50. \quad (2)$$

This relation holds when $\Phi_* < 0.39$; when $\Phi_* > 0.39$, the universal distribution is only slightly altered. With damping of the swirl, the distribution $\varphi_\Sigma = \varphi_\Sigma(\eta_\Sigma)$ approaches the universal law for axial stabilized flow in a tube; for $\Phi_* \approx 0.07$ the agreement is practically complete. For the same values of Φ_* (different eddy generators) the dependence $\varphi_\Sigma = \varphi_\Sigma(\eta_\Sigma)$ is the same for different eddy generators, which confirms that Φ_* is a universal parameter (Fig. 2). For the laminar underlayer and the transitional region, the universal distribution evidently remains the same as for axial flow; this conclusion is based on results found for other types of swirling flow [2].

Note finally an important experimental result: For the eddy generators considered, the angle of swirl changes extremely little in the flow region at the wall, in agreement with the data of [12, 13]. On the basis of this result, universal relations can be determined for the axial and rotational velocities, and an approximate method of determining the surface friction in the swirling flow can be formulated [14].

4. Intensity of the Turbulence

The turbulent properties of swirling flow characterize the general level of turbulent pulsations in the channel. The pulsation intensity is determined in the coordinate system ξ, ζ, η: ξ is taken along the direction of the total velocity, while ζ and η are perpendicular to it. Detailed information is given in [15]. Here we note only that in the range of pulsation intensities investigated all of the components are independent of the initial swirl and reach 10% at the surface and 30-35% in the axial flow region. Note that the intensity of turbulent pulsation is approximately self-modeling in Re_d; with damping of the swirl, the pulsation intensity is substantially unchanged at the wall, but decreases very markedly at the axis and is 4% at the channel outlet.

5. Integral Flow Characteristics

Information on the local parameters can be used to calculate the integral flow characteristics M, K_1, K_Σ, Φ_*, Φ, and Ω. Calculations were carried out for all the eddy generators at nine cross sections along the length of the channel. Analysis of the results shows

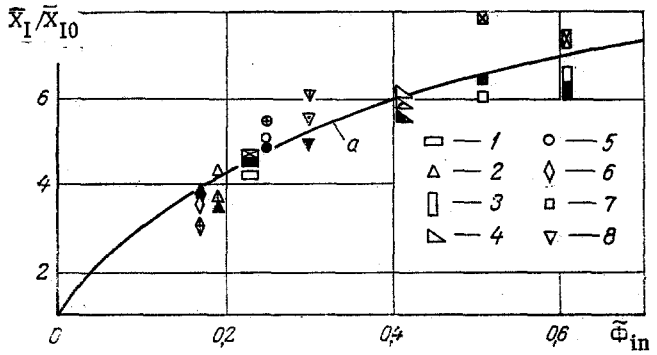

Fig. 3. Relative change in length of hydrodynamic initial section: $Re_d = 0.5 \cdot 10^5$; 1) $\varphi_I = 30°$, n = 3; 2) 15°, 3; 3) 60°, 3; 4) 45°, 3; 5) 45°, 0; 6) 45°, −1; 7) 45°, straight blades; 8) 45°, 1; a) $\bar{x}_I/\bar{x}_{I0} = 1 + 8.15\tilde{\Phi}_{*in}0.85$. The open symbols correspond to stabilization of λ_s, the filled symbols to stabilization of τ_{xw}, and the open symbols crossed by lines to stabilization of w_x.

that, in dimensionless form, the integral parameters are self-modeling in Re_d and satisfy the exponential relations

$$\begin{gathered} 0<\bar{x}<\bar{x}_1,\ \bar{M}=\exp(-m\bar{x});\ \bar{x}>\bar{x}_1,\ \bar{M}=\exp[(m_1-m)\bar{x}_1-m_1\bar{x}]; \\ \bar{x}>0,\ \bar{K}_\Sigma=\exp(-k\bar{x}); \\ 0<\bar{x}<\bar{x}_1,\ \bar{\Phi}=\exp[-(m-k)\bar{x}]; \\ \bar{x}>\bar{x}_1,\ \bar{\Phi}=\exp[(m_1-m)\bar{x}_1-(m_1-k)\bar{x}]. \end{gathered} \tag{3}$$

Numerical values of the constants m, m_1, and k are given by the equations

$$m\cdot 10^2 = 1.8 + 0.415\,\tilde{\Phi}_{*in}^{0.97};\quad m_1\cdot 10^2 = 7.82\,\tilde{\Phi}_{*in}^{1.94} - 14.25\tilde{\Phi}_{*in}^{0.94} + 9.5;$$

$$k\cdot 10^2 = -0.865\,\tilde{\Phi}_{*in}^{1.94} + 1.53\,\tilde{\Phi}_{*in}^{0.97} - 0.1,$$

and values of $\bar{x}_1$ are given in Table 1.

Analysis of the experimental data leads to an important practical relation between Φ and Φ_* for all the eddy generators in the range from 0 to $\bar{x}$ = 150:

$$\Phi = 0.427\,\Phi_*^{0.81},\quad \frac{l}{d} = 150, \tag{4}$$

and hence to the expression

$$\int_0^R Pr\,dr = (2.36\,\Phi_*^{0.19} - 1)\int_0^R \rho w_x^2\, r\,dr,$$

which may be used to solve integral momentum relations for swirling flow in tubes.

The first and second Euler theorems, written for swirling flow, yield the two equations

$$\frac{dM}{d\bar{x}} = -4\pi R^3\tau_{\varphi w};\quad \frac{dK_\Sigma}{d\bar{x}} = -4\pi R^2\tau_{xw}, \tag{5}$$

and hence it is possible to calculate the limiting swirl angle for the flow at the wall $\tan\varphi_w$ and the axial, tangential, and total coefficients of surface friction. For example, the expressions for $\tan\varphi_w$ and $c_x/2$ are as follows:

$$\operatorname{tg}\varphi_w = 0.427\,\frac{m}{k}\,\Phi_*^{0.81};\quad \frac{c_x}{2} = \frac{0.318\,k\rho K_\Sigma}{\left\{v\,\mathrm{Re}_d\left[0.95 + 1.8\,\dfrac{\Phi_*^{0.81}}{\mathrm{Re}_d^{0.12}}\right]\right\}^2}, \tag{6}$$

where the numerical value of Φ_* is determined by simultaneous solution of Eqs. (3) and (4).

6. Hydraulic Drag

The energy losses in the channel are determined using the Bernoulli equation, written for a nonuniform distribution of the local flow parameter over the channel cross section. In this case the expression for the hydraulic-drag coefficient is

$$\xi = -\frac{\Delta E}{2\pi \int_0^R \frac{\rho w_x^2}{2} w_x r dr}. \tag{7}$$

For convenience of calculation, the mean velocity distribution is chosen as the scale; the total expression for the hydraulic-drag coefficient can then be written as the sum of the individual components:

$$\xi_\Sigma = \xi_1 + \xi_2 + \xi_3. \tag{8}$$

Generalizing the experimental data for all the eddy generators yields the following equations:

$$\xi_1 = 1.89\,\tilde{\Phi}_{*\text{in}}^{0.81} - 0.29; \quad \xi_2 + \xi_3 = B\,\mathrm{Re}_d^{-q}; \quad \xi_3 = A\,\mathrm{Re}_d^{-a}; \tag{9}$$

$$\xi_1^* = 1.15\tilde{\Phi}_{*\text{in}}^{0.81} - 0.13,$$

and the numerical values of A, B, and α are given by the expressions

$$A = 23.1\tilde{\Phi}_{*\text{in}}^{-0.99}; \quad B = 18.9\tilde{\Phi}_{*\text{in}}^{-0.2}; \quad a = 7.2\cdot 10^{-2}\tilde{\Phi}_{*\text{in}}^{-0.75}. \tag{10}$$

Since the relative change in energy of the flow over the length of the channel is also exponential

$$\bar{E} = \exp(-c\bar{x}), \text{ where } c = 1.36\cdot 10^{-2}\tilde{\Phi}_{*\text{in}}^{0.43}, \tag{11}$$

it is possible to determine the hydraulic drag of the swirling flow per unit length of tube. Simple transformations give

$$\lambda_s = Bc\,\mathrm{Re}_d^{-a}\exp(-c\bar{x}), \tag{12}$$

where B, c, and α are given by Eqs. (10) and (11).

7. Length of Hydrodynamic Initial Section

This term will be understood to mean the distance from the source of swirling to the cross section at which the local and integral flow parameters take values characteristic for axial stabilized flow in the tube. The value $\bar{x}_{I_0}$ defined in [16] is taken as the scale.

Three characteristics are used in the analysis: stabilization of the hydraulic losses per unit length of tube, the tangential frictional stress at the channel wall, and the universal velocity distribution.

Results obtained for one set of flow conditions are shown in Fig. 3. Analysis of the experimental data shows that the initial swirl intensity has the greatest effect on the ratio $\bar{x}_I/\bar{x}_{I_0}$; the effect of Re_d is negligible. The generalizing equation for the range of parameter values investigated is

$$\bar{x}_I = 1.35\,\mathrm{Re}_d^{-0.25}\,[1 + (9.125 - 1.95\cdot 10^{-5}\,\mathrm{Re}_d)\,(0.427\,\tilde{\Phi}_{*\text{in}}^{0.81})^{(0.63-1.26\cdot 10^{-6}\mathrm{Re}_d)}]. \tag{13}$$

Analysis of the stabilization of the turbulent characteristics shows that the pulsation intensity corresponds to values of the axial stabilized flow over the length that are 10-20% larger than those given by Eq. (13).

NOTATION

$c_x/2 = \tau_{xw}/\rho_0 w_{x0}^2$; $d = 2R$; $E = 2\pi\int_0^R P^* w_x r dr$, energy; $\bar{E} = E/E_{in}$; G, flow rate; $\Phi_* = M/K_1 R$; $\Phi = M/K_\Sigma R$, intensity of swirl at an arbitrary cross section; $\tilde{\Phi}_{*in}$, $\tilde{\Phi}_{in}$, mean values of Φ_* and Φ at inlet; $\bar{\Phi} = \Phi/\Phi_{in}$; $\bar{\Phi}_* = \Phi_*/\Phi_{*in}$; $M = 2\pi\int_0^R \rho w_x w_\varphi r^2 dr$; $\bar{M} = M/M_{in}$; $K_1 = 2\pi\int_0^R \rho w_x^2 r dr$, axial momentum; $K_\Sigma = 2\pi\int_0^R (P + \rho w_x^2) r dr$; $\bar{K}_\Sigma = K_\Sigma/K_{\Sigma in}$; $\bar{K}_1 = K_1/K_{1in}$; $\mathrm{Re}_d = \rho u 2R/\mu$, mean-flow-rate Reynolds

number; $\bar{x} = x/2R$; x, r, φ, cylindrical coordinates; w_x, w_φ, w_Σ, axial, tangential, and total velocities; x_I, x_{Io}, lengths of hydrodynamic initial section with swirl and without it; τ_{wx}, $\tau_{\varphi w}$, $\tau_{\Sigma w}$, tangential stresses at wall; $\tan\varphi_w = \tau_{\varphi w}/\tau_{xw}$; $\varphi_\Sigma = w_\Sigma/v_\Sigma^*$; $n_\Sigma = yv_\Sigma^*/\nu$; $v_\Sigma^* = \sqrt{\tau_{\Sigma w}/\rho}$; φ, angle of swirl; φ_I, n, eddy-generator parameters; $\Omega = M\sqrt{\rho}/G\sqrt{K_\Sigma}$; $\xi_i = -\Delta E_i/0.5Gu^2$; $\xi_i^* = -\Delta E_i/0.5G_{o1}w_{o1}^2$; $\overline{\rho_{o1}w_{o1}}$, mean mass-flow-rate density in eddy-generator cross section; Δ, difference. Indices: s, swirl; eg, eddy generator; in, inlet; w, wall; 00, channel axis; I, initial; 0, maximum.

LITERATURE CITED

1. V. K. Shchukin, Heat Transfer and Hydrodynamics of Internal Flows in Fields of Mass Forces [in Russian], Mashinostroenie, Moscow (1970).
2. L. B. Reznyakov, B. P. Ustimenko, et al., Thermophysical Principles of Cyclonic Heating and Technological Processes [in Russian], Nauka, Alma-Ata (1974).
3. M. A. Gol'dshtik, Inzh.-Fiz. Zh., 2, No. 3 (1959).
4. G. E. Sturov, in: Aerodynamics [in Russian], Nauka, Novosibirsk (1973), p. 134.
5. M. F. Shnaiderman and A. N. Ershov, Inzh.-Fiz. Zh., 27, No. 4 (1975).
6. D. P. Veske and G. E. Sturov, Izv. Sibirsk. Otd. Akad. Nauk SSSR, Ser. Tekh. Nauk, 3, No. 13 (1972).
7. V. N. Kalashnikov, Yu. D. Raiskii, and L. E. Tunkel', Izv. Akad. Nauk SSSR, Mekh. Zhidk. Gaza, No. 1 (1970).
8. Kh. O. Nurste, Izv. Akad. Nauk ÉstSSR, Ser. Fiz.-Mat., 22, No. 1 (1973).
9. Wolf, Leiven, and Feidger, Raketn. Tekh. Kosmonavt., 7, No. 5 (1969).
10. R. B. Akhmedov, Teploénergetika, No. 6 (1962).
11. V. I. Goldobeev et al., Izv. Vyssh. Uchebn. Zaved., Aviats. Tekh., No. 4 (1973).
12. F. Liepe, Maschinenbautechnik, 12, No. 3 (1963).
13. V. K. Shchukin et al., in: Proceedings of the Kazan' Aviation Institute [in Russian], No. 194, Kazan' (1975), p. 26.
14. A. A. Khalatov, in: Proceedings of the Kazan' Aviation Institute [in Russian], No. 194, Kazan' (1975), p. 18.
15. V. G. Letyagin et al., Paper Deposited at VIMI, No. VMD02674 (1976).
16. S. S. Kutateladze and A. I. Leont'ev, Heat and Mass Transfer and Friction in a Turbulent Boundary Layer [in Russian], Énergiya, Moscow (1972).

STATISTICAL CHARACTERISTICS OF MASS LOST IN THERMAL DESTRUCTION

G. D. Petrov and V. L. Rovinskii

UDC 536.36:535.46

It is shown that there are characteristic pulsations of the concentration of condensed particles in the high-temperature destruction of solids in the absence of gasdynamic pressure.

The thermostability of materials under the action of a high-enthalpy flow is one of the main factors determining the efficiency of operation of much modern thermal equipment. However, many aspects of the thermal destruction of solids remain unclear; in particular, the disperse characteristics of the material produced have been inadequately studied. In calculating the efficiency of thermoprotective coatings the mass lost in the form of disperse phase is often ignored, which leads to significant errors [1, 2]. In considering ablation it is usually assumed [1, 3] that the destruction of a thermoprotective coating in a high-enthalpy flow occurs with the formation, at the surface, of a molten layer, which is then

Translated from Inzhenerno-Fizicheskii Zhurnal, Vol. 33, No. 2, pp. 233-237, August, 1977. Original article submitted June 15, 1976.